Article:
Xia, D, Yu, H, Li, Q et al. (4 more authors) (2022) Compressive and Thermally Stable Boron Nitride Aerogel as a Multifunctional Sorbent. Dalton Transactions, 51 (3). pp. 836-841. ISSN 1477-9226

https://doi.org/10.1039/d1dt02650j

Dalton Transactions

An international journal of inorganic chemistry

Accepted Manuscript

This article can be cited before page numbers have been issued, to do this please use: D. Xia, H. Yu, Q. Li, J. Mannering, R. Menzel, P. Huang and H. Li, *Dalton Trans.*, 2022, DOI: 10.1039/D1DT02650J.

ROYAL SOCIETY OF CHEMISTRY

rsc.li/dalton

View Article Online
DOI: 10.1039/D1DT02650J

COMMUNICATION

Compressive and Thermally Stable Boron Nitride Aerogel as a Multifunctional Sorbent

Received 00th January 20xx,
Accepted 00th January 20xx

DOI: 10.1039/x0xx00000x

Dong Xia[a, f], Huayang Yu[b, f], Qun Li,[c] Jamie Mannering,[a] Robert Menzel,[a] Peng Huang[d]* and Heng Li[e]*

Boron nitride (BN) aerogels are three-dimensional, bulk materials, with exceptional performances in a wide range of areas. However, detailed investigations into the relationships of synthesis, structure, and properties are rare. This study demonstrates the feasibility of tuning the performance of the aerogel by simply altering the relative amount of the precursors in the synthesis, which subsequently leads to the formation of aerogels with distinctive properties in specific surface areas, porosity, and compressibility. The utilisations of these structurally different aerogels are exemplified by investigating in a series of important industrial-related areas, such as oil absorption/desorption, direct combustion, adsorptive desulfurisation, and CO_2 capture. The study raises the prospects of BN aerogels in applications of gas-phase catalysis and thermal superinsulation materials.

Hexagonal boron nitride (BN) is a two-dimensional (2D) layered nanomaterial. It is formed by covalently-connected boron and nitrogen atoms in a honeycomb lattice, with one-atom thickness.[1, 2] BN lends itself to a broad spectrum of applications including field emitters,[3] sorbents,[4] separators,[5] and catalysts,[6] owing to the prominent features of high specific surface area,[7] excellent mechanical strength,[8] superior oxidation resistance[9] and exceptional thermal-conducting capability.[10] Previous studies are mainly focused on BN powder materials, which are fabricated by annealing the mixture of boron precursor and nitrogen precursor at a high temperature under an inert atmosphere.[11] Recently, the fabrication of macroscopic porous three-dimensional (3D) BN aerogel with tailored nanostructures has drawn great attention.[12] The unique combination of the nano- and macro-structures opens up routes in new and emerging areas, such as energy, environmental science, and bio-applications. The transformation from a 2D material to a 3D aerogel enables completely new functionalities and extends its current application range to monolithic thermal insulators,[13] bulk sorbents,[14] membranes,[15] thermal management materials,[16] phase-change materials.[17] The assembled aerogel not only maintains its excellent physicochemical properties, but also embraces additional benefits of reversible compressibility, easy regeneration after sorption, varied internal microstructures and morphologies, stretchability and twistability, and tunable pore sizes.[12, 18]

Currently, the frequently adopted route to produce BN aerogels is by using melamine and boric acid as starting materials, which offers great simplicity during fabrication.[19] Nevertheless, the physicochemical properties of these BN aerogels and their corresponding performances are largely unknown. It's well accepted for BN powder that excess nitrogen functions as 'porogen agents' which generates pores, resulting in a wide

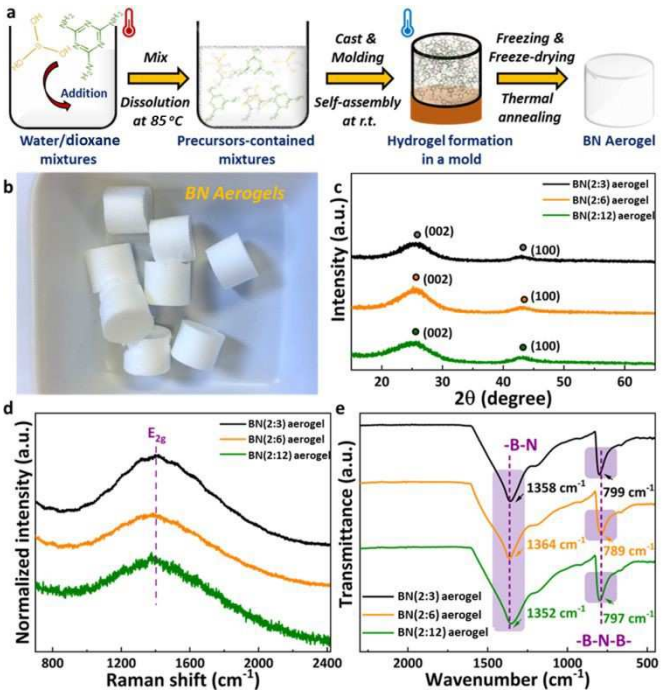

Fig. 1 (a) Schematic illustration of the preparation of the BN aerogels. (b) Digital photo of BN aerogels. (c) XRD patterns, (d) Raman spectra and (e) FT-IR spectra of different BN aerogels.

[a] School of Chemistry, University of Leeds, Leeds, LS2 9JT, UK
[b] School of Design, University of Leeds, Leeds, LS2 9JT, UK
[c] Department of Chemical and Biochemical Engineering, College of Chemistry and Chemical Engineering, Xiamen University, Xiamen 361005, China
[d] Department of Materials, University of Manchester, Manchester, M13 9PL, UK
[e] Key Laboratory of Estuarine Ecological Security and Environmental Health, Tan Kah Kee College, Xiamen University, 363105, Zhangzhou, China
[f] These authors contributed equally: Dong Xia, Huayang Yu.

Electronic Supplementary Information (ESI) available: [details of any supplementary information available should be included here]. See DOI: 10.1039/x0xx00000x

View Article Online
DOI: 10.1039/D1DT02650J

Table 1. Physical parameters of different BN aerogels.

B:N mole ratio	Density (mg/cm³)	Volume shrinkage (%)	SSA [a] (m²/g)	V_{meso} [b] (cm³/g)	V_{micro} [c] (cm³/g)	Strength [d] (at 80%, kPa)	Young's modulus [e] (Pa)	Reversible compressibility	BN layers [f] (n)
2:3	20.0	48	280	0.065	0	1.22	16.62	+	5
2:6	21.4	42	938	0.190	0.110	0.46	6.63	+	5
2:12	16.4	28	651	0.251	0.022	0.33	2.23	+	3

[a] *SSA*, specific surface area from BET measurement; [b] V_{meso}, accumulated mesopore volume; [c] V_{micro}, accumulated micropore volume; [d] *Strength*, obtained from Fig. 3d; [e] *Young's modulus*, calculated from Fig. 3d; [f] *BN layers*, analyzed from (002) characteristic peak in Fig. 1c.

variety of porosities inside the powder materials.[19] In this study, excess nitrogen was utilised as a porogen agent for the preparation of BN aerogels with controlled microstructures and properties. Specifically, three different BN aerogels with high structural integrity and uniformity were synthesised via a simple precursor self-assembly strategy. Experimental insights into the structure and properties of the BN aerogels were gained through a combination of bulk characterisation techniques. The multifunctionality of the aerogels was demonstrated by liquid-phase absorption, adsorptive desulfurization (ADS) and CO_2 capture measurements, all exhibiting high capacities and great potential for environmental remediations.

The schematic procedure for the synthesis of BN aerogels is illustrated in Fig. 1a. The two precursors of boric acid and melamine with different nominal mole ratios (4:1, 2:1, and 1:1) and the corresponding B:N mole ratios of 2:3, 2:6 and 2:12, were carefully selected to provide different loadings of nitrogen porogen. The mixtures were dissolved in water/dioxane solution at 85 °C to facilitate the dissolution and dispersion of precursors, followed by casting into customised molds (ESI Fig. S1) to form hydrogels. Subsequently, the hydrogels were freeze-dried and annealed at 1000 °C in an H_2/N_2 (5 % H_2) atmosphere to yield the desired aerogels and were named as BN(2:3) aerogel, BN(2:6) aerogel and BN(2:12) aerogel according to their mole ratios of B and N atoms in the respective precursors. The white, free-standing, cylindrical monolithic BN aerogel showed high structural integrity (Fig. 1b) and possessed a relatively low density between 16.4 and 21.4 mg/cm³ (Table 1, ESI Fig. S2). The shape change of the aerogel during fabrication is directly related to the loadings of melamine in the synthesis. Higher nitrogen content in the aerogels results in less volume shrinkage (Table 1). Taking into account the simplicity of fabrication and ease of shape control, the aerogel synthesis can be readily scaled up and fit into various bespoke molds (ESI Fig. S3).

To verify the successful synthesis of BN aerogels, bulk characterisation techniques (e.g. XRD, Raman spectroscopy and IR) were employed to elucidate the structural properties. XRD patterns of all the aerogels (Fig. 1c) showed two characteristic peaks at 25° and 43°, corresponding to the (002) and (100) basal planes, in line with reported studies.[20] Analyses along the (002) stacking direction using Bragg's law (interlayer distance) and Scherrer equation (mean crystallite domain size) indicated the formation of 5, 5 and 3 layers for the BN(2:3) aerogel, BN(2:6) aerogel and BN(2:12) aerogel, respectively (Table 1). The reduction in stacked layers for the BN(2:12) aerogel may be caused by the decomposition of the excess melamine and the evaporation of gases during the high-temperature annealing process, which promotes disordering in the stacking direction of the BN layers.[21]

The BN aerogels showed an interlayer distance in the range between 0.35 nm and 0.36 nm in the (002) basal plane, larger than that of typical bulk BN crystals (0.33 - 0.34 nm),[11] likely indicating the formation of a turbostratic morphology. All the BN aerogel samples exhibited one broad peak at around 1400 cm^{-1} in the Raman spectrum (Fig. 1d), which belongs to the stretching vibration of E_{2g}.[22] Typically, bulk hexagonal BN shows an E_{2g} vibration peak at 1367 cm^{-1} and a fixed full-width at half-maximum (FWHM) value of 9.1 cm^{-1}. Changes in the peak position and FWHM value in the Raman spectrum were often used to estimate the number of layers in the modified BN aerogel.[11] The shifting of the E_{2g} vibration peak to a higher wavenumber suggests a decrease in the crystallite domain size, while the significantly greater FWHM value (Table S2, ESI)

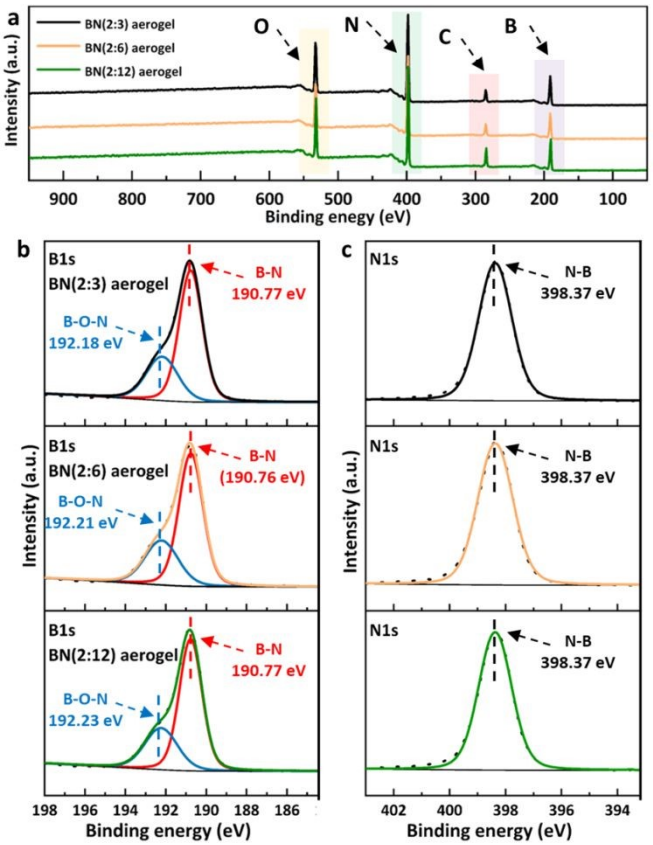

Fig. 2 (a) XPS full spectra, (b) B1s high-resolution scans and (c) N1s high-resolution scans of BN(2:3) aerogel, BN(2:6) aerogel and BN(2:12) aerogel.

indicates the generation of multi-layered BN.[11] The successful synthesis of BN was also confirmed by IR spectroscopy. All the BN aerogels showed two characteristic vibration bands originating from the in-plane B-N stretching vibration (~1373-1384 cm^{-1}) and the out-of-plane B-N-B bending vibration (~779-808 cm^{-1}).[19, 23] The characteristic B-N-B vibration band of the aerogel shifted to higher wavenumbers (blue-shift) compared with commercial BN powder (775 cm^{-1}, ESI Fig. S6), implying the enhanced bond stiffness in the aerogel.[22] X-ray photoelectron spectroscopic analysis (XPS) was conducted to determine the elemental composition and chemical binding states of the BN aerogels (Fig. 2). The XPS full spectra demonstrated the presence of only B, N, C and O elements (Fig. 2a), consistent with reported studies that adopted similar approaches to fabricate BN derived materials.[20, 24] The XPS high-resolution scans in the B1s regions and N1s regions also confirmed the successful formation of BN in the final product. Specifically, the two strong characteristic peaks located at ~192.2 eV and ~190.7 eV in Fig. 2b belong to B-O-N binding and B-N binding, respectively, consistent with reported results.[24, 25] The sharp peak in the high-resolution XPS N1s spectrum is also stemmed from the N-B binding (~398.4 eV, Fig. 2c).[25]

Nitrogen adsorption-desorption isotherms clearly showed differences for the three aerogels with various ratios of the precursors, although they all belong to type-IV hysteresis loop (Fig. 3a). The isotherm of the BN(2:3) aerogel exhibited a typical type-H3 loop, indicative of the existence of crack, plate slit-like and wedge-like pores.[26] In contrast, the BN(2:6) aerogel and BN(2:12) aerogel displayed a type-H4 loop, suggesting a combination of micropores and mesopores.[26] This was corroborated by the pore size distribution results (Fig. 3b), where the BN(2:3) aerogel was dominated by micropore structure, and the other two aerogels were hierarchical. The largest specific surface area of 938 m^2/g was observed for the BN(2:6) aerogel, followed by the BN(2:12) aerogel (651 m^2/g) and the BN(2:3) aerogel (280 m^2/g). However, the largest pore volume accumulation emerged in the BN(2:12) aerogel (0.251 cm^3/g, Table 1), which was attributed to its high mesoporosity. The results indicate that surface area and porosity of the BN aerogel can be tuned by simply altering the mole ratio of the precursors. Notably, a certain amount of nitrogen porogen will benefit the property of BN aerogels. A moderate amount of nitrogen generates a good amount of microporosity, e.g. 0.110 cm^3/g micropore volume for the BN(2:6) aerogel (Table 1); whilst too large amount reduces the microporosity and results in the creation of mesoporosity, e.g. a significantly decreased micropore volume accumulation (0.022 cm^3/g) for the BN(2:12) aerogel (Table 1).

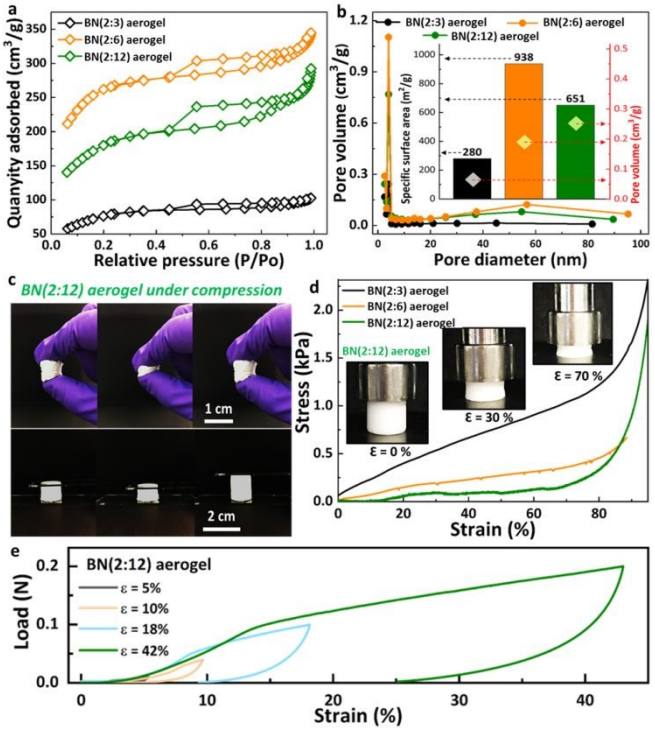

Fig. 3 (a) Nitrogen adsorption-desorption curves, (b) BJH pore size distribution, specific surface area and pore volume (inserted) of different BN aerogels. (c) BN(2:12) aerogel monolith under compression via fingers (top panel) and a glass slide (bottom panel). (d) Compression stress-strain curves of different BN aerogels. (e) Load-strain curves of BN(2:12) aerogel under different compressive strain.

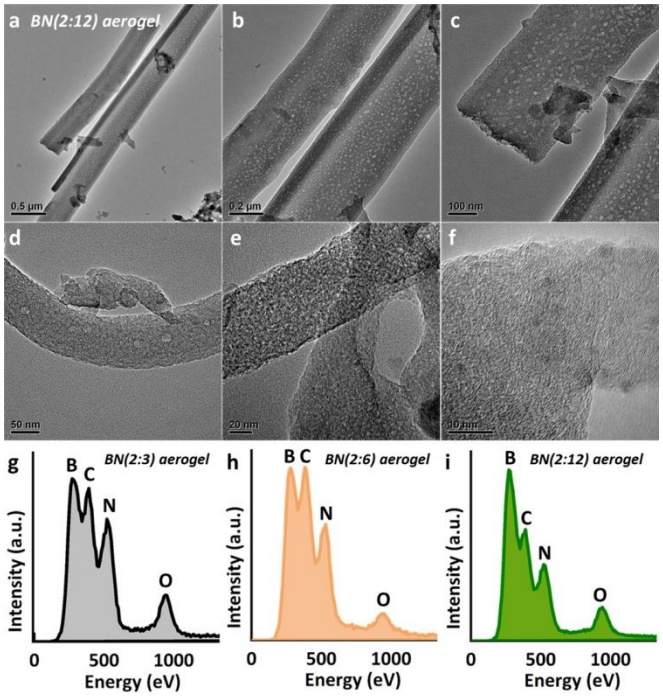

Fig. 4 TEM images of the BN nanobelts in BN(2:12) aerogel (a-f). TEM-EDX line scan analysis of BN(2:3) aerogel (g), BN(2:6) aerogel (h), and BN(2:12) aerogel (i).

The BN(2:12) aerogel was selected as a representative sample to examine the microstructures using transmission electron microscopic (TEM) analysis. The TEM micrographs of the aerogel clearly showed nanobelt-like shapes with abundant porous microstructures (mesopores) uniformly distributed on the surface of the nanobelts (Figs. 4a-4d), indicating the effectiveness of melamine as the porogen. The high-resolution TEM micrographs in Figs. 4e-4f exhibited the highly amorphous and turbostratic features of the BN nanosheets (in line with the XRD analysis), with micropores across the entire structure. The above observations were supported by the BET analyses results, where the BN(2:12) aerogel showed large volumes of mesopores and micropores. Energy-dispersive X-ray (EDX) line scans also confirmed the existence of the B, N, C and O elements in all the prepared BN aerogels (Figs. 4g-4i), consistent with the XPS survey scans.

Compression stress-strain curves showed high mechanical compressibility (up to 90 % strain) for the three aerogels (Fig. 3d), with the BN(2:12) aerogel showing the smallest Young's modulus of 2.23 Pa (Table 1). Additionally, all the BN aerogels exhibited good recoverability under different compressive strains (ESI Fig. S8), as exemplified by the BN(2:12) aerogel in Fig. 3e. The shape of the aerogel was restored immediately after the removal of applied forces, without any breakage of the monolithic aerogel structure (Fig. 3c). The mechanical performance is directly related to the composition of the aerogel (i.e. the B:N ratio). A slight excess of nitrogen leads to the formation of more covalent bonds in the aerogel structure and thus a high Young's modulus. The mechanically strong aerogel can be used in areas such as phase-change materials, where resistance to deformation is desired.[27] When large excess of porogen was used in the synthesis, the resulting aerogel became more elastic and compressible, because of higher pore volumes (exposure of more active sites) and reduced interconnectivity in the structure. The less stiff aerogel may find applications in oil sorption,[28] in which high adsorption capacity and compression ratio are advantageous.

Scanning electron microscopic analysis (SEM) implied that the long, belt-like BN crystals in the BN(2:12) aerogel were highly interconnected, with plenty of open microstructures, which contributed to the observed high compressibility and good shape recoverability (ESI Fig. S9). The evident macroporosity (1-10 microns) in the BN(2:12) aerogel is likely to enable fast kinetics of mass transfer into the aerogel interior, which is beneficial for reducing diffusion-related resistance. These results highlight the prospect of BN aerogels to be utilised as supports for catalytic gas sensors,[29] thermal superinsulation materials,[30] compressive materials,[12] sorbents,[14] etc. Moreover, the above results showed the feasibility of regulating the performance of the aerogel by altering the relative amount of precursors in the synthesis. Different ratios of B:N led to the formation of aerogels with distinctive compressibility, porosity, and specific areas, which have various implications in multiple fields.

The high thermal stability of the BN(2:12) aerogel was visualised by directly burning the aerogel using a butane torch in air (flame temperature up to approximately 1,430 °C, Fig. 5a). No

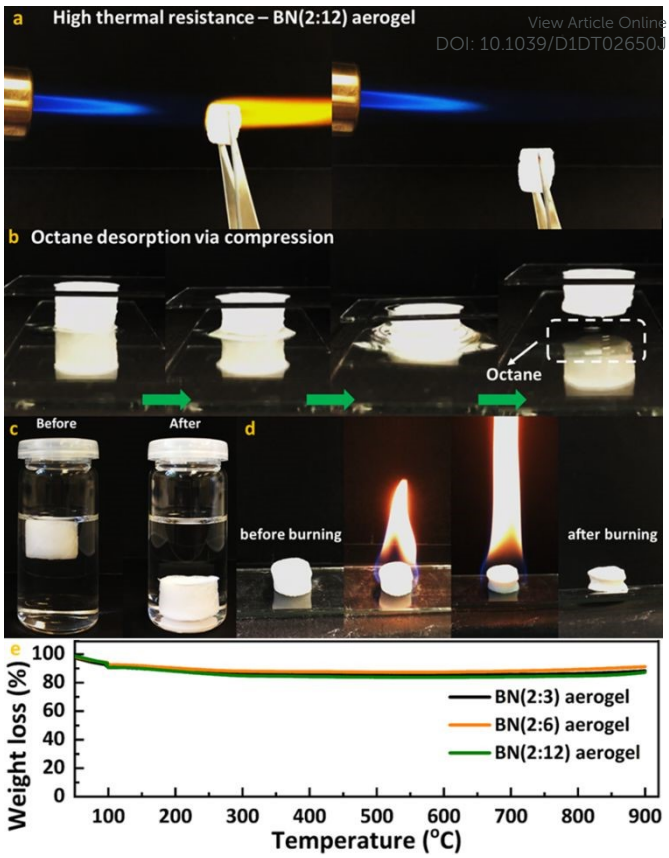

Fig. 5 Digital photos of (a) BN(2:12) aerogel under the burning of a butane torch in air, (b) BN(2:12) aerogel under a glass slide compression after octane absorption, and (c) BN(2:12) aerogel in octane solution contained sample vial, and (d) BN(2:12) aerogel combustion in air after octane desorption. (e) TGA thermograms of BN(2:3), BN(2:6), and BN(2:12) aerogels in air atmosphere.

deformation or combustion of the aerogel was observed after continuous burning for 1 minute, suggesting its exceptional thermal stability and resistance to high-temperature oxidation.[12] The hydrophobic nature of the BN aerogel makes it an ideal candidate for oil absorption. To take advantage of these characteristics, octane (an important component of gasoline) was chosen as an example to demonstrate the excellent oil absorption capacity and easy regeneration of the exhausted aerogel. Here, the BN(2:12) was selected as the model aerogel owing to its relatively large micro/mesopore pore volume and high compressibility. As shown in Fig. 5c, the aerogel settled to the bottom of the sample vial after being saturated with octane. By applying compression forces to the aerogel, the absorbed oil can be conveniently recovered and stored for other purposes (Fig. 5b). Repeated cycles showed no compromise in the oil absorption capacity and mechanical performance of the aerogel. Complete removal of the residual oil can be easily achieved by burning the spent aerogel at a high temperature (Fig. 5d), owing to its excellent thermal stability.[31] Thermal gravimetric analysis (TGA, Fig. 5e) further confirmed the high thermal stability of the aerogel under heating of up to 900 °C in air atmosphere. This prominent feature highlights the promise of BN aerogel to be exploited in important industrial applications such as oil leakage treatment.

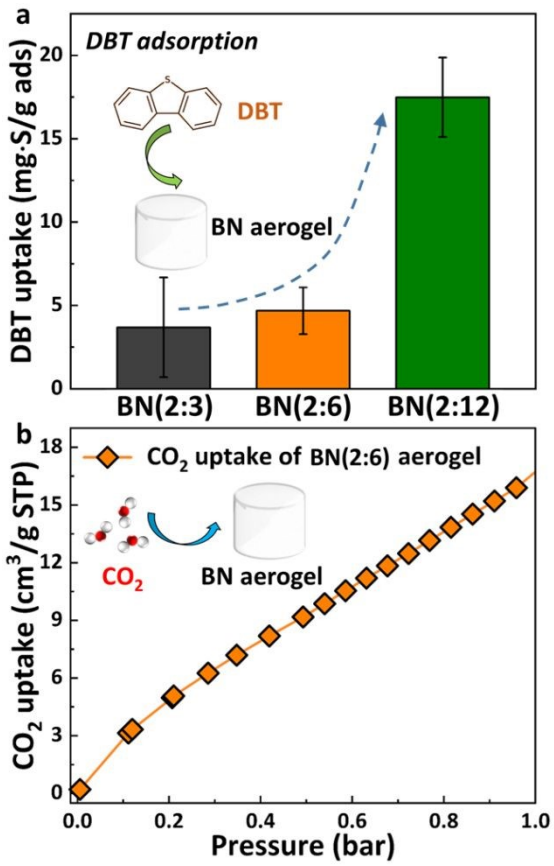

Fig. 6 (a) DBT uptake capacity of BN aerogels. (b) CO_2 uptake capacity of the BN(2:6) aerogel at 298 K.

In order to demonstrate the liquid-phase adsorption capacity of the BN aerogel, dibenzothiophene (DBT, a typical sulfur-containing component in fuels) was chosen to investigate the adsorptive desulfurization (ADS) performance in octane solutions. The BN(2:12) aerogel exhibited the highest DBT uptake capacity of 17.5 mg·S/g ads, because of its ample mesopores and hierarchical porosities (i.e. micropores connected to a large fraction of mesopores) in the structure that facilitate mass transfer and expose more active sites for sorption (Fig. 6a) than the other two BN aerogels.[19] The adsorbed DBT molecules were strongly bonded to the BN active sites via S···B=N- binding, namely strong Lewis acid-base interactions.[23] The adsorption of DBT molecules onto the BN aerogel was supported by the appearance of a new absorption vibration band at 740 cm^{-1} in the IR spectrum (ESI Fig. S11). Similarly, the adsorbed DBT can be removed via thermal treatment at 400 °C (ESI Fig. S11), for which the aerogel exhibits great potential for re-use due to its high thermal and mechanical stability. Considering its large specific surface area and micropore volume, the BN(2:6) aerogel was taken forward to investigate the industrially important CO_2 adsorption. The CO_2 uptake capacity of the aerogel increased when the pressure rises (up to 1 bar), with the maximum uptake capacity of 0.76 mmol/g achieved at equilibrium (Fig. 6b), displaying promising CO_2 capture capability at room temperature via physisorption.

In summary, BN aerogels with tunable physicochemical properties were fabricated via controlling the mole ratios (i.e. different degrees of nitrogen excess) of the precursors, which results in discrepancies in the number of BN layers, surface area, pore size distribution and compressibility. More specifically, an ideal B:N ratio balances the compromise between micro-pore/surface area generation and interconnectivity/mechanical properties. All the BN aerogels exhibited high oil absorption capacities and thermal stability, which enable this type of material to be used in applications such as oil leakage treatment, combustion medium, and high-temperature insulating materials. Furthermore, the BN aerogels showed good performance in both adsorptive desulfurization and CO_2 capture. Further enhancement of the sorption capacity of the aerogel can be seen by tailoring the surface area, porosity, alkalinity and hybridisation. The introduction of electric-conducting properties into BN aerogels (i.e. incorporation of nanocarbon-based conductive materials) would also dramatically widen their current application range.

Conflicts of interest

There are no conflicts to declare.

Acknowledgements

This research was sponsored by the China Scholarship Council and the University of Leeds. The research of H. Li was supported by the National Key R&D Program of China (2019YFC1805801) and the National Natural Science Foundation of China (22038012).

Notes and references

1. A. Nag, K. Raidongia, K. P. S. S. Hembram, R. Datta, U. V. Waghmare and C. N. R. Rao, *ACS Nano*, 2010, **4**, 1539-1544.
2. W. Luo, Y. Wang, E. Hitz, Y. Lin, B. Yang and L. Hu, *Adv. Funct. Mater.*, 2017, **27**, 1701450.
3. T. Vogl, M. W. Doherty, B. C. Buchler, Y. Lu and P. K. Lam, *Nanoscale*, 2019, **11**, 14362-14371.
4. T. Liu, Y.L. Li, J.Y. He, Y. Hu, C.M. Wang, K.S. Zhang, X.J. Huang, L.-T. Kong and J.H. Liu, *New J. Chem.*, 2019, **43**, 3280-3290.
5. Y. Fan, D. Liu, M. M. Rahman, T. Tao, W. Lei, S. Mateti, B. Yu, J. Wang, C. Yang and Y. Chen, *ACS Appl. Energy Mater.*, 2019, **2**, 2620-2628.
6. P. Wu, W. Zhu, Y. Chao, J. Zhang, P. Zhang, H. Zhu, C. Li, Z. Chen, H. Li and S. Dai, *Chem. Commun.*, 2016, **52**, 144-147.
7. S. Marchesini, C. M. McGilvery, J. Bailey and C. Petit, *ACS Nano*, 2017, **11**, 10003-10011.
8. T. Tian, J. Hou, H. Ansari, Y. Xiong, A. L'Hermitte, D. Danaci, R. Pini and C. Petit, *J. Mater. Chem. A*, 2021, **9**, 13366-13373.
9. Y. Wang, L. Xu, Z. Yang, H. Xie, P. Jiang, J. Dai, W. Luo, Y. Yao, E. Hitz, R. Yang, B. Yang and L. Hu, *Nanoscale*, 2018, **10**, 167-173.
10. Q. Weng, X. Wang, X. Wang, Y. Bando and D. Golberg, *Chem. Soc. Rev.*, 2016, **45**, 3989-4012.
11. Q. Weng, X. Wang, C. Zhi, Y. Bando and D. Golberg, *ACS Nano*, 2013, **7**, 1558-1565.
12. G. Li, M. Zhu, W. Gong, R. Du, A. Eychmüller, T. Li, W. Lv and X. Zhang, *Adv. Funct. Mater.*, 2019, **29**, 1900188.
13. J. Wang, D. Liu, Q. Li, C. Chen, Z. Chen, P. Song, J. Hao, Y. Li, S. Fakhrhoseini, M. Naebe, X. Wang and W. Lei, *ACS Nano*, 2019, **13**, 7860-7870.

View Article Online
DOI: 10.1039/D1DT02650J

14. Y. Song, B. Li, S. Yang, G. Ding, C. Zhang and X. Xie, *Sci. Rep.*, 2015, **5**, 10337.
15. C. Chen, J. Wang, D. Liu, C. Yang, Y. Liu, R. S. Ruoff and W. Lei, *Nat. Commun.*, 2018, **9**, 1902.
16. Z. Liang, Y. Pei, C. Chen, B. Jiang, Y. Yao, H. Xie, M. Jiao, G. Chen, T. Li, B. Yang and L. Hu, *ACS Nano*, 2019, **13**, 12653-12661.
17. B. Wang, G. Li, L. Xu, J. Liao and X. Zhang, *ACS Nano*, 2020, **14**, 16590-16599.
18. W. Lei, V. N. Mochalin, D. Liu, S. Qin, Y. Gogotsi and Y. Chen, *Nat. Commun.*, 2015, **6**, 8849.
19. J. Xiong, L. Yang, Y. Chao, J. Pang, M. Zhang, W. Zhu and H. Li, *ACS Sustain. Chem. Eng.*, 2016, **4**, 4457-4464.
20. J. Xiong, W. Zhu, H. Li, L. Yang, Y. Chao, P. Wu, S. Xun, W. Jiang, M. Zhang and H. Li, *J. Mater. Chem. A*, 2015, **3**, 12738-12747.
21. C. Gautam, C. S. Tiwary, S. Jose, G. Brunetto, S. Ozden, S. Vinod, P. Raghavan, S. Biradar, D. S. Galvao and P. M. Ajayan, *ACS Nano*, 2015, **9**, 12088-12095.
22. A. Pakdel, X. Wang, C. Zhi, Y. Bando, K. Watanabe, T. Sekiguchi, T. Nakayama and D. Golberg, *J. Mater. Chem.*, 2012, **22**, 4818-4824.
23. J. Xiong, W. Zhu, H. Li, W. Ding, Y. Chao, P. Wu, S. Xun, M. Zhang and H. Li, *Green Chem.*, 2015, **17**, 1647-1656.
24. C. Yang, J. Wang, Y. Chen, D. Liu, S. Huang and W. Lei, *Nanoscale*, 2018, **10**, 10979-10985.
25. I. Esteve-Adell, J. He, F. Ramiro, P. Atienzar, A. Primo and H. García, *Nanoscale*, 2018, **10**, 4391-4397.
26. S. Fu, Q. Fang, A. Li, Z. Li, J. Han, X. Dang and W. Han, *Energy Sci. Eng.*, 2021, **9**, 80-100.
27. M. Wang, T. Zhang, D. Mao, Y. Yao, X. Zeng, L. Ren, Q. Cai, S. Mateti, L. H. Li, X. Zeng, G. Du, R. Sun, Y. Chen, J.B. Xu and C.P. Wong, *ACS Nano*, 2019, **13**, 7402-7409.
28. C. Chen, F. Li, Y. Zhang, B. Wang, Y. Fan, X. Wang and R. Sun, *Chem. Eng. J.*, 2018, **350**, 173-180.
29. A. Harley-Trochimczyk, T. Pham, J. Chang, E. Chen, M. A. Worsley, A. Zettl, W. Mickelson and R. Maboudian, *Adv. Funct. Mater.*, 2016, **26**, 433-439.
30. X. Xu, Q. Zhang, M. Hao, Y. Hu, Z. Lin, L. Peng, T. Wang, X. Ren, C. Wang, Z. Zhao, C. Wan, H. Fei, L. Wang, J. Zhu, H. Sun, W. Chen, T. Du, B. Deng, G. J. Cheng, I. Shakir, C. Dames, T. S. Fisher, X. Zhang, H. Li, Y. Huang and X. Duan, *Science*, 2019, **363**, 723.
31. J. Han, G. Du, W. Gao and H. Bai, *Adv. Funct. Mater.*, 2019, **29**, 1900412.